

Supporting Information for
“Factors controlling Hadley circulation changes from the Last Glacial
Maximum to the end of the 21st century”

Roberta D’Agostino^{1,2,3}

Piero Lionello^{2,3}

Ori Adam^{4,5}

Tapio Schneider^{4,6}

¹Max Planck Institute for Meteorology, Hamburg, Germany.

²DiSTeBA, University of Salento, Lecce, Italy.

³Euro-Mediterranean Center on Climate Change, Lecce, Italy.

⁴Geological Institute, ETH Zurich, Switzerland.

⁵Hebrew University, Jerusalem, Israel

⁶California Institute of Technology, Pasadena, California, USA

Contents

1. Introduction
2. Hadley Circulation in the Mid-Holocene
3. Figure S1
4. Figure S2
5. Figure S3
6. Figure S4
7. Table S1

Introduction

Here, we provide figures in support of the results discussed in the main text. Figure S1 supports the statements about the influence of the inter-hemispheric thermal contrast

Corresponding author: Roberta D’Agostino, Max Planck Institute for Meteorology, Bundesstr. 53, 20146, Hamburg, Germany, roberta.dagostino@mpimet.mpg.de

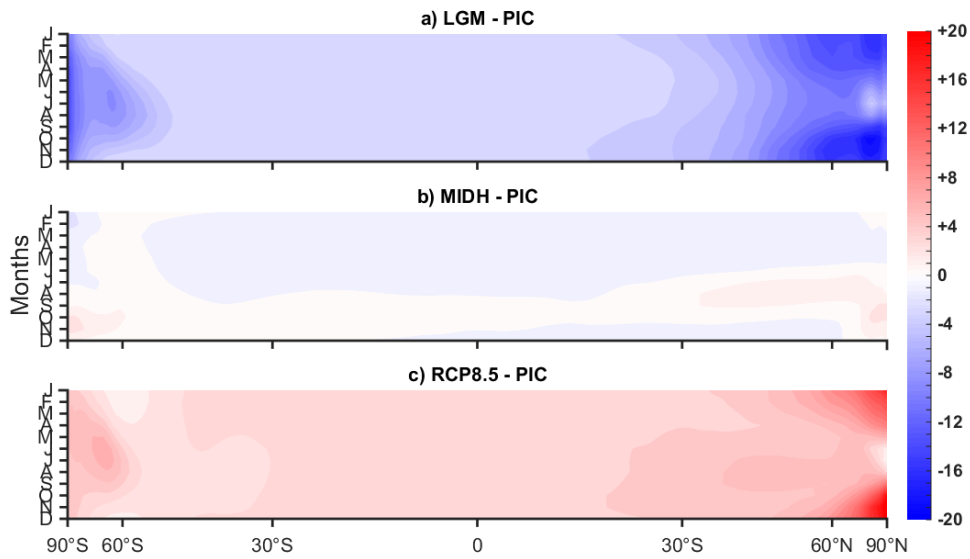


Figure S1: Seasonal cycle of the zonal mean surface air temperature difference from LGM (upper panel), MIDH (middle panel), and RCP8.5 (lower panel) to PIC. The contour interval is 1 K.

on the HC extent and strength. Figure S2 and S3 show details about the regression fits for the set of simulations, giving information about their scatter: each number represents a model according to Table S1. Additionally, Fig. S4 shows summer regressions between the HC and $\langle TT \rangle$. Results about summer do not differ substantially from winter, except for the NH extent: the regression in Figure S4a shows a contraction toward the equator of the NH HC as the climate warms. It is largely a result of seasonality changes, shown in Figure 2, which are themselves related to a tendency for a delayed retreat of the northern hemisphere summer monsoons under global warming [Kitoh *et al.*, 2013].

Moreover, the following section includes a short description of HC behavior in the MIDH simulations. MIDH is the most different experiment in the set because of the changed orbital parameters, leading to substantial changes of the atmospheric circulations (Figure 2).

Hadley Circulation in the Mid-Holocene

The HC response in the MIDH differs substantially from both LGM and RCP8.5, as a result of the orbital parameter change (Figure 2). In MIDH, the NH in summer receives

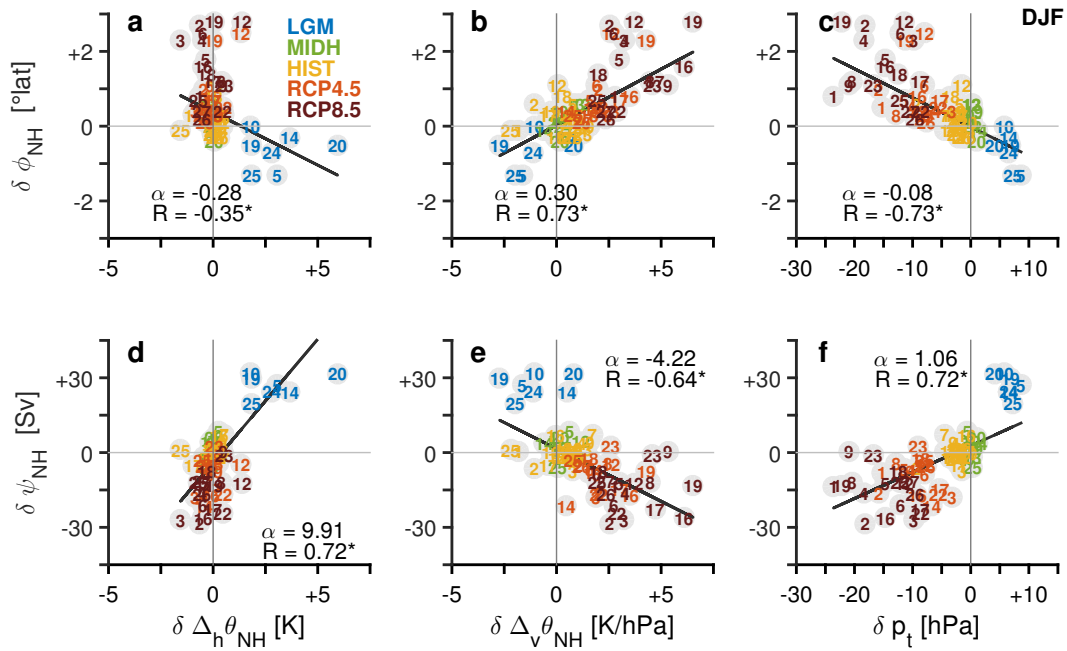


Figure S2: Scatter plots between winter values of ϕ_{NH} (upper row) and ψ_{NH} (lower row) versus $\Delta_h \theta_{\text{NH}}$, $\Delta_v \theta_{\text{NH}}$, and p_t . Each value represents the difference to the corresponding PIC value. Experiments are identified by different colors, according to the legend in (a). Each model is marked with a number, as in Table S1. Robust regression lines are shown in black. Regression coefficients (α) and correlation coefficients (R) are indicated inside each panel. Statistically significant correlations (5% significance level, Student t -test) are indicated by an asterisk.

additional insolation, with a corresponding reduction in the SH. This leads to a reduction of the meridional temperature contrast in the NH and to a stronger inter-hemispheric thermal contrast than other experiments (Figure S1), with very little change in the annual global or tropical mean temperature. Generally speaking, in the LGM (the coldest climate considered), the HC strengthens and contracts toward the equator, while in RCP8.5 (the warmest climate), the HC shows an opposite response (Figure 2). By contrast, the MIDH HC changes substantially compared with other experiments, as shown also by *Merlis et al. [2013]* in idealized simulations. *Merlis et al. [2013]* showed that when perihelion occurs in the summer of a hemisphere with a subtropical continent, changes in the top-of-atmosphere energy balance, together with a poleward shift of the monsoonal circulation boundary, lead to a strengthening of the monsoonal circulation. We find a similar JJA shift of the atmospheric circulation toward the warmer (northern) hemisphere, with an

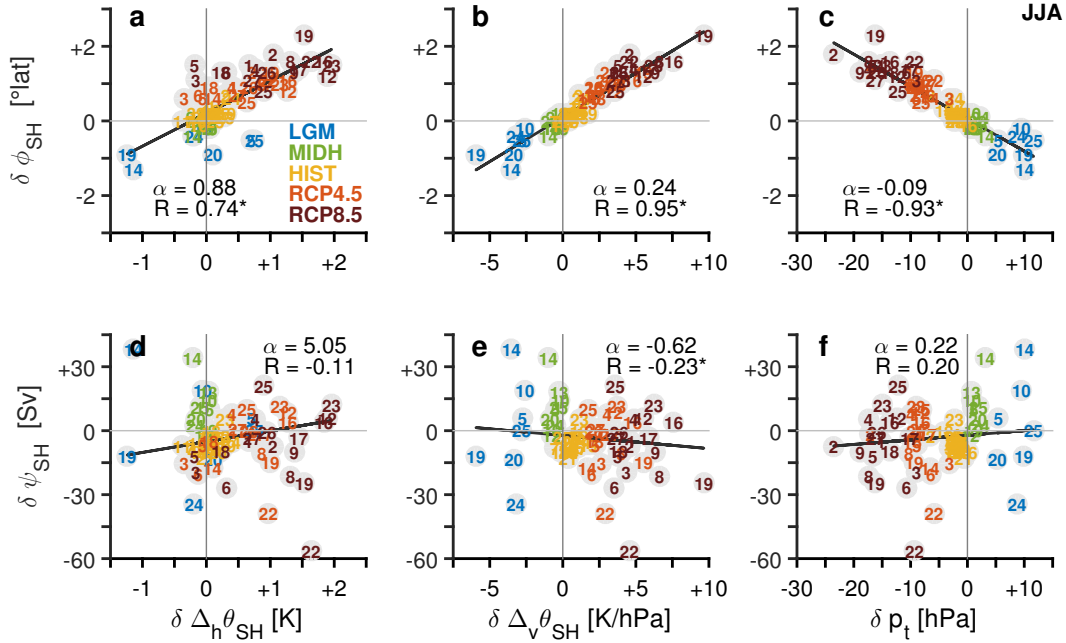


Figure S3: Scatter plots between winter values of ϕ_{SH} (upper row) and ψ_{SH} (lower row) versus $\Delta_h \theta_{SH}$, $\Delta_v \theta_{SH}$, and p_t . Plotting conventions as in Fig. S2.

associated strengthening and northward migration of the HC ascending branch and ITCZ, and with a strengthening and widening of the cross-equatorial winter (southern) HC. The warming of the NH relative to the SH leads to substantial changes in the strength of the HC; changes in the inter-hemispheric thermal contrast, in the meridional temperature gradient within a hemisphere, and in the static stability and tropopause height may all play roles in these HC strength variations.

References

- Kitoh, A., H. Endo, K. Krishna Kumar, I. F. Cavalcanti, P. Goswami, and T. Zhou (2013), Monsoons in a changing world: a regional perspective in a global context, *Journal of Geophysical Research: Atmospheres*, 118(8), 3053–3065.
- Merlis, T. M., T. Schneider, S. Bordoni, and I. Eisenman (2013), Hadley circulation response to orbital precession. part ii: Subtropical continent, *Journal of Climate*, 26(3), 754–771.

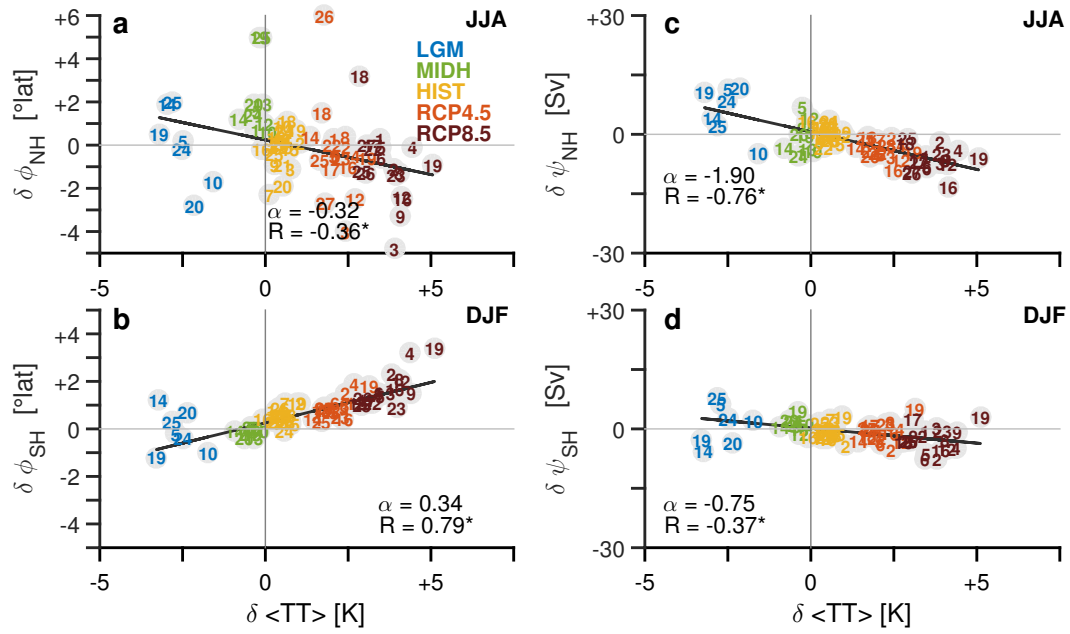


Figure S4: Scatter plots between summer values of (a) ϕ_{NH} , (b) ϕ_{SH} , (c) ψ_{NH} , and (d) ψ_{SH} , all versus $\langle TT \rangle$, averaged between $30^{\circ}S$ and $30^{\circ}N$. Plotting conventions as in Fig. S2.

Stocker, T. F., D. Qin, G.-K. Plattner, M. Tignor, S. K. Allen, J. Boschung, A. Nauels, Y. Xia, V. Bex, and P. M. Midgley (2014), *Climate change 2013: The physical science basis*.

Table S1: List of PMIP3 and CMIP5 models for each experiment in this study: Last Glacial Maximum (LGM), Mid-Holocene (MIDH), Pre-Industrial Control (PIC), Historical (HIST), Representative Concentration Pathways (RCP 4.5 and 8.5) from r1i1p1 ensemble [Stocker *et al.*, 2014].

	Models	Resolution	LGM	MIDH	PIC	HIST	RCP 4.5	RCP 8.5
1	bcc-csm1-1	$T42 \times 26$		x	x	x	x	x
2	bcc-csm1-1-m	$T106 \times 26$			x	x	x	x
3	BNU-ESM	$T42 \times 26$			x	x	x	x
4	CanESM2	$T63 \times 35$			x	x	x	x
5	CCSM4	$288 \times 192 \times 27$	x	x	x	x	x	x
6	CESM1-CAM5	$288 \times 192 \times 27$			x		x	x
7	CMCC-CESM	$T31 \times 39$			x	x		
8	CMCC-CM	$T159 \times 31$			x		x	x
9	CMCC-CMS	$T63 \times 95$			x	x		x
10	CNRM-CM5	$T127 \times 31$	x	x	x	x		
11	CNRM-CM5-2	$T127 \times 31$			x	x		
12	CSIRO-Mk3-6-0	$T63 \times 35$		x	x	x	x	x
13	CSIRO-Mk3L-1-2	$T63 \times 18$		x	x			
14	FGOALS-g2	$T42 \times 26$	x	x	x	x	x	
15	FIO-ESM	$T42 \times 26$			x	x		
16	GFDL-CM3	$144 \times 90 \times 48$			x	x	x	x
17	GFDL-ESM2M	$144 \times 90 \times 24$			x	x	x	x
18	inmcm4	$180 \times 120 \times 21$			x	x	x	x
19	IPSL-CM5A-LR	$96 \times 96 \times 39$	x	x	x	x	x	x
20	MIROC-ESM	$T42 \times 80$	x	x	x	x		
21	MIROC-ESM-CHEM	$T42 \times 80$			x	x		
22	MIROC5	$T85 \times 40$			x	x	x	x
23	MPI-ESM-MR	$T63 \times 95$			x	x	x	x
24	MPI-ESM-P	$T63 \times 47$	x	x	x	x		
25	MRI-CGCM3	$T159 \times 48$	x	x	x	x	x	x
26	NorESM1-M	$144 \times 96 \times 26$			x	x	x	x
27	NorESM1-ME	$144 \times 96 \times 26$			x	x	x	x